Rapid hyperpolarization and purification of the metabolite fumarate in aqueous solution

Stephan Knecht[a], John W. Blanchard[b], Danila Barskiy[c], Eleonora Cavallari[d], Laurynas Dagys[e], Erik Van Dyke[c], Maksim Tsukanov[c], Bea Bliemel[c], Kerstin Münnemann[f], Silvio Aime[d], Francesca Reineri[d], Malcolm H. Levitt[e], Gerd Buntkowsky[a], Alexander Pines[c], Peter Blümler[g], Dmitry Budker[b,g], James Eills[b,g,*]

a) Eduard-Zintl-Institute for Inorganic Chemistry and Physical Chemistry, Technical University Darmstadt, 64287 Darmstadt, Germany
b) Helmholtz-Institut Mainz, GSI Helmholtzzentrum für Schwerionenforschung GmbH, 55128 Mainz, Germany
c) Department of Chemistry, University of California, Berkeley, U.S.A.
d) Dept. of Molecular Biotechnology and Health Sciences, University of Torino, Torino, Italy
e) University of Southampton, Southampton, United Kingdom
f) Technical University of Kaiserslautern, Kaiserslautern, Germany
g) Johannes Gutenberg University, D-55090 Mainz, Germany
(*) Correspondence: eills@uni-mainz.de

Abstract: Hyperpolarized fumarate is a promising agent for carbon-13 magnetic resonance metabolic imaging of cellular necrosis. Molecular imaging applications require nuclear hyperpolarization to attain sufficient signal strength. Dissolution dynamic nuclear polarization is the current state-of-the-art methodology for hyperpolarizing fumarate, but this is expensive and relatively slow. Alternatively, this important biomolecule can be hyperpolarized in a cheap and convenient manner using parahydrogen-induced polarization. However, this process requires a chemical reaction, and the resulting hyperpolarized fumarate solutions are contaminated with the catalyst, unreacted reagents, and reaction side product molecules, and are hence unsuitable for use *in vivo*. In this work we show that the hyperpolarized fumarate can be purified from these contaminants by acid precipitation as a pure solid, and later redissolved at a chosen concentration in a clean aqueous solvent. Significant advances in the reaction conditions and reactor equipment allow us to form hyperpolarized fumarate at a concentration of several hundred millimolar, at ^{13}C polarization levels of 30-45%.

Introduction

Nuclear magnetic resonance (NMR) and magnetic resonance imaging (MRI) are analytical techniques used to extract information about the structure or composition of a sample noninvasively. Unfortunately these methods are rather insensitive, and in order to overcome the limitations this imposes, hyperpolarization methods have been developed to produce samples with enhanced magnetic resonance signals. Signal enhancements in the order of 10^5 can be achieved for solution-state samples using hyperpolarization techniques such as dissolution dynamic nuclear polarization (dDNP)[1,2] or parahydrogen-induced polarization (PHIP) [3–5]. This allows the injection of hyperpolarized probe molecules *in vivo*, and subsequent imaging of metabolism[6–10]. One such example is the imaging of hyperpolarized fumarate, which is converted to malate in one step of the Krebs cycle, and acts as a sensitive probe of cell necrosis[11–18]. This has been demonstrated in preclinical MRI studies as e.g. a method to study tumour response to therapy[11] and image acute kidney injury[15] and myocardial infarction[17].

For preclinical studies the currently preferred method to hyperpolarize fumarate is dDNP, but polarization build-up times in the order of an hour are typical, and the expense and high technical demands of this method strongly limit its widespread application[19]. We recently showed that hyperpolarized fumarate can be formed via PHIP[20,21], which is advantageous since it is much easier to implement, and 1-2 orders of magnitude less expensive than dDNP[2,4]. A molecular precursor is chemically reacted with hydrogen gas enriched in the *para* nuclear spin isomer, and this is followed by a magnetic field cycle[22,23] to transfer the *para* spin order from the hydrogen nuclei to the ^{13}C nucleus in fumarate. It is necessary to polarize the ^{13}C nucleus for *in vivo* imaging because the hyperpolarized ^{13}C nuclei relax back to thermal equilibrium slower than ^{1}H nuclei, and have a large chemical shift dispersion which allows chemical selectivity. The drawback to producing hyperpolarized fumarate via PHIP is that, in addition to the desired fumarate product, the reaction solutions contain a plethora of additional chemicals; most notably the ruthenium catalyst, unreacted reagents, and reaction side product molecules.

In this work we demonstrate that PHIP-polarized fumarate solutions can be purified of contaminants by acid precipitation of the fumarate as a solid, and subsequent redissolution of the pure material in a clean aqueous solvent. This physicochemical manipulation is possible because the solubility of fumarate is significantly reduced in acidic solution[24]. We perform the hydrogenation reaction in a steel reactor, which allows us to work with high hydrogen flow rates, and hence form hyperpolarized fumarate at higher concentrations than was demonstrated in previous work[21]. This makes PHIP competitive with dDNP for the production of nuclear spin-polarized fumarate, since we show that it can be formed in higher concentrations and with higher ^{13}C polarization.

Signal enhancement or polarization level alone does not indicate the total signal intensity available from the hyperpolarized species, which for many applications is a crucial parameter. We define as the key figure of merit *molar polarization*, which we take as the product of the carbon-13 polarization times the concentration of [1-^{13}C]fumarate molecules. For *in vitro* or *in vivo* studies using hyperpolarized biomolecules, important criteria for the solutions prior to injection/perfusion are[25]: (1) the concentration of the hyperpolarized species; (2) the polarization level (usually >10% is desirable); (3) purity from toxic contaminants, and; (4) the biocompatibility of the solution, i.e. being at physiological pH, temperature, and osmolarity. In this paper we will address these points in the context of our work forming fumarate via PHIP.

Results

To produce hyperpolarized fumarate, para-enriched hydrogen gas was rapidly bubbled through a precursor solution in a heated steel reactor. The sample was then ejected into a magnetically shielded chamber, and a magnetic field cycle was used to transfer the ^{1}H singlet order in fumarate (originating from the parahydrogen protons) into ^{13}C magnetisation of the carboxylate carbon. In experiments involving a purification step, part of this solution was mixed with a concentrated sodium fumarate solution (to raise the overall fumarate concentration), and then mixed with HCl which lowered the pH and caused fumaric acid to precipitate out of solution. The residual reaction solution was filtered off and the fumaric acid crystals were redissolved in aqueous solution. The precipitation and redissolution steps were carried out in a 100 mT Halbach permanent magnet array to preserve the hyperpolarized spin order throughout. Unless otherwise stated, experiments were performed without isotopic enrichment of the precursor molecule, and the ~2.2% of molecules containing a ^{13}C spin in the carboxylate position were observed in the NMR experiments. A schematic showing the chemical reaction and experimental apparatus is shown in Fig. 1. Further experimental details are provided in the Materials and Methods.

Optimizing molar polarization

Since it is important to produce hyperpolarized fumarate in high concentration and with high ^{13}C polarization, we performed the chemical reaction with varied bubbling duration to find an optimum. In each experiment, after the chemical reaction and magnetic field cycle, the ^{13}C-polarized fumarate solution was transferred to a benchtop NMR spectrometer for ^{13}C signal acquisition using a $\pi/2$ pulse. After the hyperpolarized NMR signals had relaxed, a thermal equilibrium ^{1}H NMR spectrum was acquired on each sample to quantify the fumarate concentration. The results of these experiments are shown in Fig. 2a, and further experimental details are provided in the Materials and Methods section. The concentration of fumarate increases approximately linearly with bubbling duration up to 150 mM after 60 s, but the rate of fumarate formation seems to slow beyond this, and 180 mM is produced after 90 s. The polarization decreases as bubbling duration is increased due to nuclear spin relaxation of the fumarate ^{1}H singlet state.

In Fig. 2b we show the molar polarization assuming [1-^{13}C]-labelled material, which effectively scales the molar polarization by a factor of ~50 relative to the unlabelled case.

Purification of hyperpolarized fumarate

To test precipitation/redissolution as a method to purify hyperpolarized fumarate solutions, the same reaction and field cycle procedure was used as before, with a 60 s bubbling duration chosen as it led to formation of a high concentration of fumarate (150 mM) at a relatively high polarization level. After performing the reaction and magnetic field cycle, the ^{13}C-polarized fumarate solution was split into a control sample and a sample that was purified. The purified solution was transported to the benchtop NMR spectrometer for signal acquisition following a $\pi/2$ pulse. Immediately following this, the control sample was measured in the same manner. For both samples, after the hyperpolarized NMR signals had fully relaxed, a thermal equilibrium ^{1}H NMR spectrum was acquired to quantify the fumarate concentration. The time between sample ejection from the reactor and detecting ^{13}C spectra of the purified and control samples was approximately 30 s and 34 s, respectively. Further experimental details are provided in the Materials and Methods section.

To quantify the polarization level we compare a ^{13}C spectrum of a hyperpolarized sample that underwent the purification procedure, and a thermal equilibrium ^{13}C spectrum of a 500 mM [1-^{13}C]fumarate sample (isotopically enriched). Both spectra were acquired using a $\pi/2$ pulse and the results are shown in Fig. 2c. From this comparison, and knowing the concentrations of fumarate in the purified and control samples, we are able to calculate that the polarization of the hyperpolarized fumarate molecules (63 mM) in the purified sample was 25%. The total fumarate concentration in the purified sample was 354 mM, due to the addition of unpolarized fumarate molecules to aid in fast precipitation. The addition of unpolarized fumarate is not necessary for the purification step, but speeds up the rate of precipitation which is convenient for this preliminary demonstration.

To compare the ^{13}C T_1 times of the purified and control samples, a modified version of the experiment was used, where instead of applying a 90° flip angle pulse, 10° flip angle pulses were used to excite the ^{13}C signals for acquisition once every 5 s. By using a small flip angle pulse, the hyperpolarization was not significantly perturbed for each signal acquisition, and the longitudinal relaxation time (T_1) of the carboxylate ^{13}C spins could be measured directly from the signal decay. The results of this experiment are shown in Fig. 2d. The ^{13}C T_1 was measured to be 86 s for the control sample, and 71 s for the purified sample. This small difference is likely due to the samples containing different concentrations of paramagnetic oxygen; the control sample was thoroughly oxygen degassed, but the aqueous solvent used to redissolve the purified fumarate was not. These T_1 values are similar to those reported in the literature[26].

As specified before, *in vivo* applications require high purity material. However, due to finite spin relaxation times it is important that the purification step is rapid, and that there is no significant polarization loss during the purification procedure (due to possible rapid relaxation effects). To investigate this, the experiment was repeated three times, and in each case we compare the ^{13}C polarization level of the control sample to the purified sample; the results are shown in Fig. 3a. We can expect slight polarization loss in the purified samples as compared to the control samples due to the shorter T_1 of the purified sample in the solution state prior to signal acquisition. However, within the given errors there is no evidence that the phase transitions have any effect on nuclear spin polarization.

For completeness, one experiment was performed in which the purification procedure was performed outside the magnet, and as expected the ^{13}C polarization was lost. The loss of nuclear magnetization when precipitating the sample in a low magnetic field is not yet fully understood. The loss of hyperpolarization could be associated with rapid spin relaxation processes in low magnetic field for the small suspended particles involved in the nucleation process, or efficient contact between the Zeeman and dipolar orders in the solid state at low magnetic field.

Fumarate metabolism

A sample of hyperpolarized fumarate was generated as

previously described, but with 20% [1-^{13}C] isotopic enrichment of the starting material. After sample precipitation, the fumarate was redissolved in a phosphate buffer, and the resulting solution was mixed with fumarase enzyme. The ^{13}C NMR signals were acquired every 7 s using 15° flip angle pulses to monitor the enzyme-catalyzed conversion of fumarate to malate, and the results are shown in Fig. 3b+c. Further experimental details are given in the Materials and Methods section. The hyperpolarized [1-^{13}C]fumarate signal at 175.4 ppm can be seen to decay, and two additional resonances corresponding to [1-^{13}C]malate and [4-^{13}C]malate appear at 181.8 and 180.6 ppm, respectively. At first the malate signals grow in intensity as the initial rate of metabolism is high, and then decay predominantly due to nuclear spin relaxation.

Quantifying contamination

To quantify how effectively the precipitation/redissolution procedure excluded the catalyst molecules from the solutions, inductively coupled plasma – optical emission spectrometry (ICP-OES) elemental analysis was performed on a purified sample. The standard procedure was used to purify the fumarate, but with an additional washing step; while on the sinter, the solid fumarate powder was washed twice with deionized water, and twice with acetone to remove residual catalyst solution from the surface of the crystals The catalyst concentration in the final solution was determined by ICP-MS to be 16 µM, which corresponds to a reduction from the initial concentration of more than 99.5%.

Thermal equilibrium ^{13}C NMR spectra were acquired of the control and purified solutions in an 11.7 T magnet. The 1024-scan spectra were acquired with ^{1}H decoupling, using a pre-scan delay of 30 s and 30° flip angle pulses. The results qualitatively show contamination of the unpurified solution with the acetylene dicarboxylate starting material and unassigned reaction side products, but no contaminants are visible in the purified sample spectrum. From these spectra, we can set an upper bound on the concentration of starting material in the purified solution at 0.6 mM, which corresponds to less than 0.4% of the fumarate concentration. Thermal equilibrium ^{1}H NMR spectra of the control and purified samples are included in the Supporting Information, which show contaminant molecules at a level of less than 1% compared to the fumarate concentration. Additionally, high-performance liquid chromatography (HPLC) spectra were acquired of the control and purified samples, and this data is included in the Supporting Information.

Discussion

We propose the unit *molar polarization*, which is a useful measure of the signal one might expect from a hyperpolarized sample in a fixed-volume detector. This is more comprehensive than reporting signal enhancement or polarization alone, which can in many hyperpolarization experiments be improved by using lower and lower substrate concentrations[27], without increasing the observable NMR signal. We report 50 mM molar polarization (assuming [1-^{13}C] isotopic enrichment of the starting material) from the control samples which used a 60 s hydrogenation reaction. For the purification step the hyperpolarized reaction samples were mixed with a 1 M sodium fumarate solution to raise the overall fumarate concentration, and speed up the rate of precipitation. This diluted the concentration of *hyperpolarized* fumarate molecules, and hence reduced the molar polarization to 16 mM. This was a convenient method for achieving fast precipitation in this initial demonstration, but is not expected to be necessary for future experiments. With higher parahydrogen pressures, fumarate can be formed in higher concentrations on a similar timescale, and at concentrations of ~200 mM or higher the precipitation is fast. Additional experimental steps such as performing the precipitation at lower temperature and optimizing the volume of acid added should aid in direct precipitation of hyperpolarized fumarate from the reaction solution.

The residual ruthenium catalyst concentration in a 1 mL purified fumarate solution was 16 µM. For comparison, the phase extraction used for preclinical experiments with PHIP-polarized pyruvate produces solutions contaminated with ~30 µM residual rhodium catalyst[9]. The toxicity of other ruthenium(II) complexes has been investigated in mice and the LD_{50} was found to be >2000 mg kg^{-1}[28], and the IC_{50} in human nontumour breast cells was found to be 1-20 µM[29]. These results indicate that the purity of our solutions from the catalyst should allow for *in vitro* and preclinical studies since the bolus of hyperpolarized solution will be further diluted in the blood. It will be necessary to investigate the toxicity of the catalyst, precursor, and reaction side product molecules, which are currently unknown.

Catalyst scavenging has been demonstrated as a way to purify hyperpolarized solutions of the catalyst molecules[30,31]. Using physicochemical manipulations to purify the target molecule from solution as demonstrated here has a number of notable advantages: (1) it is in principle a much faster chemical process, meaning less polarization is lost due to relaxation; (2) the target molecule can be purified of all contaminants, rather than only the catalyst molecules; (3) the dissolution solution can be chosen to yield a final solution at physiological conditions, and; (4) the pure material can be redissolved at an arbitrary concentration, up to its solubility limit, which can lead to significantly higher molar polarization in the final solution.

In this work we achieve ^{13}C polarization levels higher than those reported for dDNP experiments, although we note that dDNP could produce fumarate solutions with higher molar polarization since the [1,4-$^{13}C_2$]-isotopomer can be used with both carbons in principle polarized up to 100%. When fumarate is formed from parahydrogen, the proton singlet state can be converted into 100% polarization of the ^{13}C spin in the [1-^{13}C] isotopomer (an AA'X spin system), or 50% polarization of each ^{13}C spin in the [1,4-$^{13}C_2$] isotopomer (an AA'XX' spin system)[32].

In conclusion, we have demonstrated that hyperpolarized [1-^{13}C]fumarate can be formed in hundreds of millimolar concentrations via PHIP, with typical ^{13}C polarization levels of 30-45%. We show that acid precipitation as a pure solid and subsequent redissolution as a salt is an effective method to purify the hyperpolarized [1-^{13}C]fumarate from toxic contaminants in the chemical reaction solution, and that there is no measurable polarization loss caused by the precipitation and redissolution to within the measurement error. The method presented here is demonstrated on fumarate because it rapidly precipitates in acidic solution; we hope that exploiting the physicochemical properties of other molecules might allow for the purification of alternative hyperpolarized targets.

As a next step, since the ^{13}C T_1 in the solid state significantly exceeds the solution-state ^{13}C T_1 of ~70 s, systematic studies of the hyperpolarization lifetime in a precipitated state are certainly warranted[24].

Materials and Methods

Preparation and Equipment
The precursor solution for all experiments was 250 mM acetylene dicarboxylic acid monopotassium salt, 250 mM sodium sulphite and 7 mM ruthenium catalyst $[RuCp^*(CH_3CN)_3]PF_6$ in D_2O, which was prepared by dissolving the solids with heating and sonication. The solution additionally contained 250 mM NaOH, to be equimolar with the starting material. The sodium sulphite is added to increase the rate of reaction as discussed in Ref. [20]. Oxygen was removed from the solution by bubbling nitrogen through for 5 minutes. All chemicals were purchased from Sigma Aldrich.

All NMR experiments (unless otherwise stated) were performed in a 1.4 T ^1H-^{13}C dual resonance SpinSolve NMR system (Magritek, Aachen, Germany).

Parahydrogen at >99% enrichment was generated by passing hydrogen gas (>99.999% purity) over a hydrated iron oxide catalyst in a cryostat operating at 25 K (Advanced Research Systems, Macungie, U.S.A.).

For the magnetic field sweep, an MS-2 magnetic shield (Twinleaf LLC, Princeton, U.S.A.) was used to provide a 10^5 shielding factor against external magnetic fields. No static shim fields were required, since the residual field within the shield was on the order of 1 nT. The time-dependent applied magnetic field was generated from the built-in B_y shim coil, with current supplied by a Kea2 spectrometer with 1 µs time precision.

A home-built Halbach magnet array was used to provide a 100 mT static magnetic field over a cylindrical region in space of 22 mm radius and length 150 mm in which the precipitation and redissolution procedure was carried out. This was achieved by arranging two rings of 8 0.5×0.5×2 inch neodymium N52 magnets (1.4 T remanence) in a cylindrical Halbach dipole array, with the magnet centers lying on a circle of radius 45 mm.

The reactor was constructed of stainless steel with an internal volume of 20 mL, as shown in Fig. 1. 1/8 in. O.D. PEEK (polyether ether ketone) tubing was used to flow the para-enriched hydrogen gas, and 1/16 in. O.D. 0.5 mm I.D. PTFE (polytetrafluoroethylene) capillaries were used for all solution flow. These tubes were connected to the reactor via 1/4-28 PEEK fittings (part numbers P-249 and P-349, IDEX LLC, Oak Harbor, U.S.A.), and to the gas flow-control manifold via Swagelok fittings (Swagelok, Frankfurt, Germany). The reactor was wrapped in two heater mats (part number 798-3753, RS Components, Corby, U.K.), and these were connected to a power supply, with the current set to heat the reactor to 85°C.

Hydrogenation and field sweep
For all hydrogenation experiments, a 2 mL aliquot of precursor sample was loaded into the reactor via syringe injection, and given ~10 s to reach 85°C. The reactor was sealed, and parahydrogen was bubbled into the reaction solution at approximately 6 L/min for a time (60 s unless otherwise specified) at a pressure of 8.5 bar. The flow rate was set by a needle valve at the outlet of the gas manifold. After bubbling, the sample was pneumatically ejected through a PTFE capillary into a 10 mm NMR tube in the magnetic shield underneath by manually opening a two-way microfluidic valve. In order to prevent the sample from passing through any fields that could lead to undesired state-mixing during sample transport in/out of the shield, a penetrating solenoid was used to provide a 10 µT guiding field. Upon landing in the 10 mm NMR tube, a 2 s magnetic field cycle from 50 nT to 1 µT was applied. 0.6 mL of the solution was extracted through a 1/16 inch PTFE capillary into a syringe, and this was the 'control' sample.

Purification procedure
In experiments involving precipitation/redissolution, 1.25 mL of the sample in the 10 mm NMR tube was extracted into a syringe containing 0.75 mL of 1 M sodium fumarate in D_2O. The remaining 150 µL of reaction solution was lost as droplets in the transfer capillaries and containers. The 2 mL sample was then rapidly injected into 1 mL of 12 M HCl at room temperature on a glass sinter (grade 4) atop a vacuum flask. Fumaric acid crystals immediately precipitated out as a white solid. The residual solution was removed by vacuum filtration, and the fumaric acid crystals were redissolved in 1 mL of 3 M NaOD to produce the 'purified' sample.

Enzyme experiments
For the experiment to observe enzymatic conversion to malate, after the purification procedure, 450 µL of the purified sample was injected into a 5 mm NMR tube containing 10 µL of fumarase enzyme in 150 µL of pH 7 phosphate buffer solution. The NMR tube was immediately inserted into the benchtop magnet for ^{13}C signal acquisition using 15° flip angle pulses every 7 s to monitor the hyperpolarized NMR signals over time.

Acknowledgements
This project has received funding from the European Union's Horizon 2020 research and innovation programme under the Marie Skłodowska-Curie Grant Agreement No. 766402, the European Research Council (786707-FunMagResBeacons), by the European Union's Horizon 2020 Research and Innovation Program under FETOPEN grant agreement no. 858149, and Compagnia di San Paolo (Athenaeum Research 2016, n. CSTO164550). Gerd Buntkowsky gratefully acknowledges financial support by the German Research Council (DFG) under contracts BU 911/22-2 and BU 911/29-1. Kerstin Münnemann acknowledges the research unit NanoKat at the TU Kaiserslautern for financial support. Danila Barskiy acknowledges support from the National Science Foundation under grant agreement number CHE-1709944. The authors thank Kevin Herr and Lorenz Rösler (TU Darmstadt) for the HPLC measurements.

References

(1) Ardenkjær-Larsen, J. H.; Fridlund, B.; Gram, A.; Hansson, G.; Hansson, L.; Lerche, M. H.; Servin, R.; Thaning, M.; Golman, K. Increase in Signal-to-Noise Ratio of > 10,000 Times in Liquid-State NMR. *Proc. Natl. Acad. Sci.* **2003**, *100* (18), 10158–10163. https://doi.org/10.1073/pnas.1733835100.

(2) Ardenkjaer-Larsen, J. H. On the Present and Future of Dissolution-DNP. *J. Magn. Reson.* **2016**, *264*, 3–12. https://doi.org/10.1016/j.jmr.2016.01.015.

(3) Bowers, C. R.; Weitekamp, D. P. Parahydrogen and Synthesis Allow Dramatically Enhanced Nuclear Alignment. *J. Am. Chem. Soc.* **1987**, *109* (18), 5541–5542. https://doi.org/10.1021/ja00252a049.

(4) Kovtunov, K. V.; Pokochueva, E. V.; Salnikov, O. G.; Cousin, S. F.; Kurzbach, D.; Vuichoud, B.; Jannin, S.; Chekmenev, E. Y.; Goodson, B. M.; Barskiy, D. A.; Koptyug, I. V. Hyperpolarized NMR Spectroscopy: D-DNP, PHIP, and SABRE Techniques. *Chem. – Asian J.* **2018**, *13* (15), 1857–1871. https://doi.org/10.1002/asia.201800551.

(5) Hövener, J.-B.; Pravdivtsev, A. N.; Kidd, B.; Bowers, C. R.; Glöggler, S.; Kovtunov, K. V.; Plaumann, M.; Katz-Brull, R.; Buckenmaier, K.; Jerschow, A.; Reineri, F.; Theis, T.; Shchepin, R. V.; Wagner, S.; Bhattacharya, P.; Zacharias, N. M.; Chekmenev, E. Y. Parahydrogen-Based Hyperpolarization for Biomedicine. *Angew. Chem. Int. Ed.* **2018**, *57* (35), 11140–11162. https://doi.org/10.1002/anie.201711842.

(6) Nelson, S. J.; Kurhanewicz, J.; Vigneron, D. B.; Larson, P. E. Z.; Harzstark, A. L.; Ferrone, M.; Criekinge, M. van; Chang, J. W.; Bok, R.; Park, I.; Reed, G.; Carvajal, L.; Small, E. J.; Munster, P.; Weinberg, V. K.; Ardenkjaer-Larsen, J. H.; Chen, A. P.; Hurd, R. E.; Odegardstuen, L.-I.; Robb, F. J.; Tropp, J.; Murray, J. A. Metabolic Imaging of Patients with Prostate Cancer Using Hyperpolarized [1-13C]Pyruvate. *Sci. Transl. Med.* **2013**, *5* (198), 198ra108-198ra108. https://doi.org/10.1126/scitranslmed.3006070.

(7) Kurhanewicz, J.; Vigneron, D. B.; Ardenkjaer-Larsen, J. H.; Bankson, J. A.; Brindle, K.; Cunningham, C. H.; Gallagher, F. A.; Keshari, K. R.; Kjaer, A.; Laustsen, C.; Mankoff, D. A.; Merritt, M. E.; Nelson, S. J.; Pauly, J. M.; Lee, P.; Ronen, S.; Tyler, D. J.; Rajan, S. S.; Spielman, D. M.; Wald, L.; Zhang, X.; Malloy, C. R.; Rizi, R. Hyperpolarized 13C MRI: Path to Clinical Translation in Oncology. *Neoplasia N. Y. N* **2019**, *21* (1), 1–16. https://doi.org/10.1016/j.neo.2018.09.006.

(8) Wang, Z. J.; Ohliger, M. A.; Larson, P. E. Z.; Gordon, J. W.; Bok, R. A.; Slater, J.; Villanueva-Meyer, J. E.; Hess, C. P.; Kurhanewicz, J.; Vigneron, D. B. Hyperpolarized 13C MRI: State of the Art and Future Directions. *Radiology* **2019**, *291* (2), 273–284. https://doi.org/10.1148/radiol.2019182391.

(9) Cavallari, E.; Carrera, C.; Sorge, M.; Bonne, G.; Muchir, A.; Aime, S.; Reineri, F. The 13 C Hyperpolarized Pyruvate Generated by ParaHydrogen Detects the Response of the Heart to Altered Metabolism in Real Time. *Sci. Rep.* **2018**, *8* (1), 8366. https://doi.org/10.1038/s41598-018-26583-2.

(10) Cavallari, E.; Carrera, C.; Di Matteo, G.; Bondar, O.; Aime, S.; Reineri, F. In-Vitro NMR Studies of Prostate Tumor Cell Metabolism by Means of Hyperpolarized [1-13C]Pyruvate Obtained Using the PHIP-SAH Method. *Front. Oncol.* **2020**, *10*. https://doi.org/10.3389/fonc.2020.00497.

(11) Gallagher, F. A.; Kettunen, M. I.; Hu, D.-E.; Jensen, P. R.; Zandt, R. in 't; Karlsson, M.; Gisselsson, A.; Nelson, S. K.; Witney, T. H.; Bohndiek, S. E.; Hansson, G.; Peitersen, T.; Lerche, M. H.; Brindle, K. M. Production of Hyperpolarized [1,4-13C2]Malate from [1,4-13C2]Fumarate Is a Marker of Cell Necrosis and Treatment Response in Tumors. *Proc. Natl. Acad. Sci.* **2009**, *106* (47), 19801–19806. https://doi.org/10.1073/pnas.0911447106.

(12) Jensen, P. R.; Peitersen, T.; Karlsson, M.; Zandt, R. in 't; Gisselsson, A.; Hansson, G.; Meier, S.; Lerche, M. H. Tissue-Specific Short Chain Fatty Acid Metabolism and Slow Metabolic Recovery after Ischemia from Hyperpolarized NMR in Vivo. *J. Biol. Chem.* **2009**, *284* (52), 36077–36082. https://doi.org/10.1074/jbc.M109.066407.

(13) Witney, T. H.; Kettunen, M. I.; Hu, D. -e; Gallagher, F. A.; Bohndiek, S. E.; Napolitano, R.; Brindle, K. M. Detecting Treatment Response in a Model of Human Breast Adenocarcinoma Using Hyperpolarised [1- 13 C]Pyruvate and [1,4- 13 C 2]Fumarate. *Br. J. Cancer* **2010**, *103* (9), 1400–1406. https://doi.org/10.1038/sj.bjc.6605945.

(14) Bohndiek, S. E.; Kettunen, M. I.; Hu, D.; Witney, T. H.; Kennedy, B. W. C.; Gallagher, F. A.; Brindle, K. M. Detection of Tumor Response to a Vascular Disrupting Agent by Hyperpolarized 13C Magnetic Resonance Spectroscopy. *Mol. Cancer Ther.* **2010**, *9* (12), 3278–3288. https://doi.org/10.1158/1535-7163.MCT-10-0706.

(15) Clatworthy, M. R.; Kettunen, M. I.; Hu, D.-E.; Mathews, R. J.; Witney, T. H.; Kennedy, B. W. C.; Bohndiek, S. E.; Gallagher, F. A.; Jarvis, L. B.; Smith, K. G. C.; Brindle, K. M. Magnetic Resonance Imaging with Hyperpolarized [1,4-13C2]Fumarate Allows Detection of Early Renal Acute Tubular Necrosis. *Proc. Natl. Acad. Sci.* **2012**, *109* (33), 13374–13379. https://doi.org/10.1073/pnas.1205539109.

(16) Mignion, L.; Dutta, P.; Martinez, G. V.; Foroutan, P.; Gillies, R. J.; Jordan, B. F. Monitoring Chemotherapeutic Response by Hyperpolarized 13C-Fumarate MRS and Diffusion MRI. *Cancer Res.* **2014**, *74* (3), 686–694. https://doi.org/10.1158/0008-5472.CAN-13-1914.

(17) Miller, J. J.; Lau, A. Z.; Nielsen, P. M.; McMullen-Klein, G.; Lewis, A. J.; Jespersen, N. R.; Ball, V.; Gallagher, F. A.; Carr, C. A.; Laustsen, C.; Bøtker, H. E.; Tyler, D. J.; Schroeder, M. A. Hyperpolarized [1,4-13C2]Fumarate Enables Magnetic Resonance-Based Imaging of Myocardial Necrosis. *JACC Cardiovasc. Imaging* **2018**, *11* (11), 1594–1606. https://doi.org/10.1016/j.jcmg.2017.09.020.

(18) Laustsen, C.; Nielsen, P. M.; Qi, H.; Løbner, M. H.; Palmfeldt, J.; Bertelsen, L. B. Hyperpolarized [1,4- 13 C]Fumarate Imaging Detects Microvascular Complications and Hypoxia Mediated Cell Death in Diabetic Nephropathy. *Sci. Rep.* **2020**, *10* (1), 9650. https://doi.org/10.1038/s41598-020-66265-6.

(19) Ardenkjaer-Larsen, J. H. Introduction to Dissolution DNP: Overview, Instrumentation, and Human Applications. In *eMagRes*; American Cancer Society, 2018; pp 63–78. https://doi.org/10.1002/9780470034590.emrstm1549.

(20) Ripka, B.; Eills, J.; Kouřilová, H.; Leutzsch, M.; Levitt, M. H.; Münnemann, K. Hyperpolarized Fumarate via Parahydrogen. *Chem. Commun.* **2018**, *54* (86), 12246–12249. https://doi.org/10.1039/C8CC06636A.

(21) Eills, J.; Cavallari, E.; Carrera, C.; Budker, D.; Aime, S.; Reineri, F. Real-Time Nuclear Magnetic Resonance Detection of Fumarase Activity Using Parahydrogen-Hyperpolarized [1-13C]Fumarate. *J. Am. Chem. Soc.* **2019**, *141* (51), 20209–20214. https://doi.org/10.1021/jacs.9b10094.

(22) Jóhannesson, H.; Axelsson, O.; Karlsson, M. Transfer of Para-Hydrogen Spin Order into Polarization by Diabatic Field Cycling. *Comptes Rendus Phys.* **2004**, *5* (3), 315–324. https://doi.org/10.1016/j.crhy.2004.02.001.

(23) Eills, J.; Blanchard, J. W.; Wu, T.; Bengs, C.; Hollenbach, J.; Budker, D.; Levitt, M. H. Polarization Transfer via Field Sweeping in Parahydrogen-Enhanced Nuclear

Magnetic Resonance. *J. Chem. Phys.* **2019**, *150* (17), 174202. https://doi.org/10.1063/1.5089486.
(24) Eills, J.; Alonso-Valdesueiro, J.; Salazar Marcano, D. E.; Ferreira da Silva, J.; Alom, S.; Rees, G. J.; Hanna, J. V.; Carravetta, M.; Levitt, M. H. Preservation of Nuclear Spin Order by Precipitation. *ChemPhysChem* **2018**, *19* (1), 40–44. https://doi.org/10.1002/cphc.201701189.
(25) Golman, K.; Petersson, J. S. Metabolic Imaging and Other Applications of Hyperpolarized 13C1. *Acad. Radiol.* **2006**, *13* (8), 932–942. https://doi.org/10.1016/j.acra.2006.06.001.
(26) Eldirdiri, A.; Clemmensen, A.; Bowen, S.; Kjær, A.; Ardenkjær-Larsen, J. H. Simultaneous Imaging of Hyperpolarized [1,4-13C2]Fumarate, [1-13C]Pyruvate and 18F–FDG in a Rat Model of Necrosis in a Clinical PET/MR Scanner. *NMR Biomed.* **2017**, *30* (12), e3803. https://doi.org/10.1002/nbm.3803.
(27) Knecht, S.; Pravdivtsev, A. N.; Hövener, J.-B.; Yurkovskaya, A. V.; Ivanov, K. L. Quantitative Description of the SABRE Process: Rigorous Consideration of Spin Dynamics and Chemical Exchange. *RSC Adv.* **2016**, *6* (29), 24470–24477. https://doi.org/10.1039/C5RA28059A.
(28) Mello-Andrade, F.; Cardoso, C. G.; Silva, C. R. e; Chen-Chen, L.; Melo-Reis, P. R. de; Lima, A. P. de; Oliveira, R.; Ferraz, I. B. M.; Grisolia, C. K.; Almeida, M. A. P.; Batista, A. A.; Silveira-Lacerda, E. de P. Acute Toxic Effects of Ruthenium (II)/Amino Acid/Diphosphine Complexes on Swiss Mice and Zebrafish Embryos. *Biomed. Pharmacother.* **2018**, *107*, 1082–1092. https://doi.org/10.1016/j.biopha.2018.08.051.
(29) dos Santos, E. R.; Graminha, A. E.; Schultz, M. S.; Correia, I.; Selistre-de-Araújo, H. S.; Corrêa, R. S.; Ellena, J.; Lacerda, E. de P. S.; Pessoa, J. C.; Batista, A. A. Cytotoxic Activity and Structural Features of Ru(II)/Phosphine/Amino Acid Complexes. *J. Inorg. Biochem.* **2018**, *182*, 48–60. https://doi.org/10.1016/j.jinorgbio.2017.12.010.
(30) Kidd, B. E.; Gesiorski, J. L.; Gemeinhardt, M. E.; Shchepin, R. V.; Kovtunov, K. V.; Koptyug, I. V.; Chekmenev, E. Y.; Goodson, B. M. Facile Removal of Homogeneous SABRE Catalysts for Purifying Hyperpolarized Metronidazole, a Potential Hypoxia Sensor. *J. Phys. Chem. C* **2018**, *122* (29), 16848–16852. https://doi.org/10.1021/acs.jpcc.8b05758.
(31) Barskiy, D. A.; Ke, L. A.; Li, X.; Stevenson, V.; Widarman, N.; Zhang, H.; Truxal, A.; Pines, A. Rapid Catalyst Capture Enables Metal-Free Para-Hydrogen-Based Hyperpolarized Contrast Agents. *J. Phys. Chem. Lett.* **2018**, *9* (11), 2721–2724. https://doi.org/10.1021/acs.jpclett.8b01007.
(32) Levitt, M. H. Symmetry Constraints on Spin Dynamics: Application to Hyperpolarized NMR. *J. Magn. Reson.* **2016**, *262*, 91–99. https://doi.org/10.1016/j.jmr.2015.08.021.

Figures

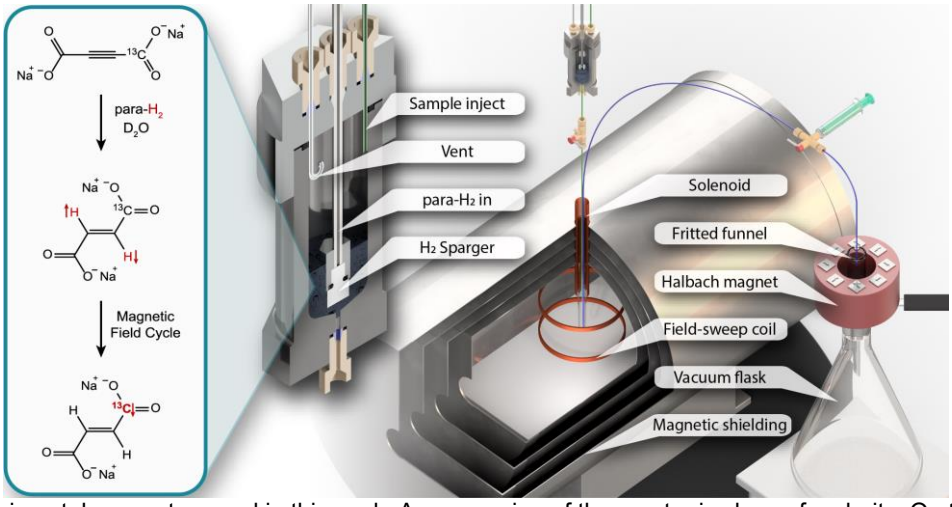

Fig. 1: The experimental apparatus used in this work. An expansion of the reactor is shown for clarity. On the left the chemical reaction and magnetic field cycle step are shown, with red arrows and atom labels representing the hyperpolarized nuclei.

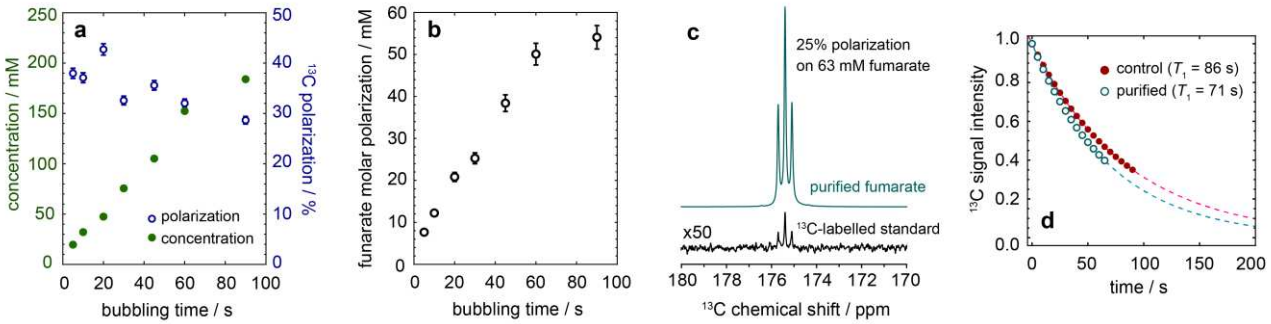

Fig. 2: (a) The polarization and concentration of [1-^{13}C]fumarate formed for different durations of parahydrogen bubbling, under the experimental conditions described in the text. (b) Molar polarization of [1-^{13}C]fumarate, i.e. the product of concentration and polarization. (c) ^{13}C NMR spectra of a purified hyperpolarized fumarate solution (at natural ^{13}C abundance) and a standard solution of 500 mM [1-^{13}C]fumarate with thermal equilibrium spin polarization. Both spectra were acquired using one transient, and are shown with 0.3 Hz line broadening. (d) ^{13}C T_1 data for the control and purified samples. Each data point shows the integral of the [1-^{13}C]fumarate resonance in the corresponding spectrum. The ^{13}C signal intensity in both datasets is normalized to 1 for the first data point, and the dotted lines are monoexponential decays of the form e^{-t/T_1}, fit to the data using the stated T_1 values.

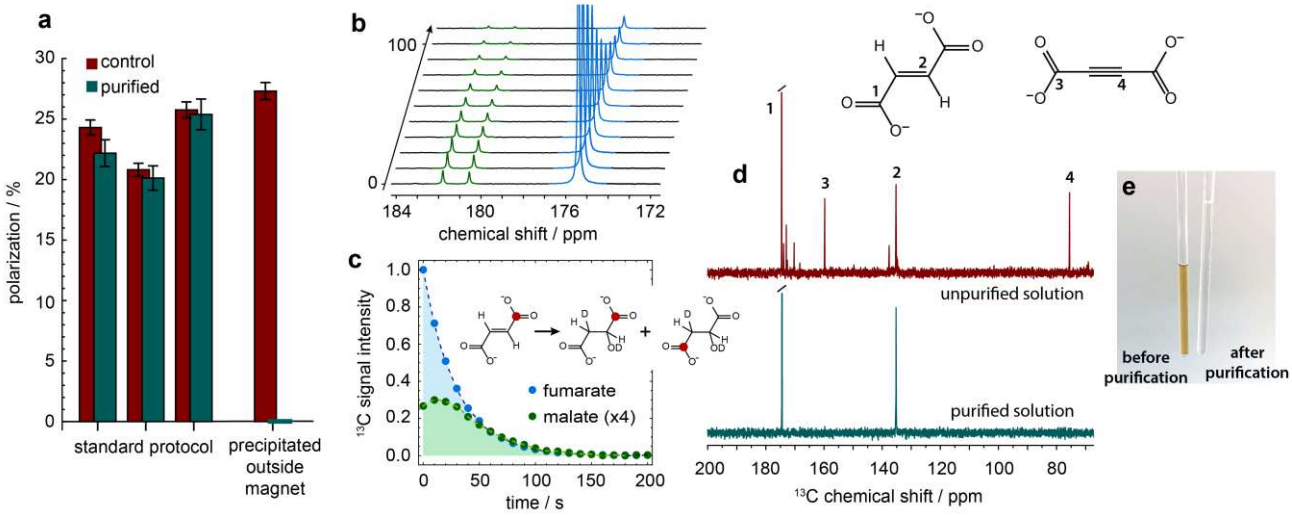

Fig. 3: (a) The polarization of the hyperpolarized [1-^{13}C]fumarate molecules for the experiments described in the text. Systematic errors are shown by the error bars. (b) A series of ^{13}C NMR spectra of a purified hyperpolarized fumarate solution after addition to a phosphate buffer solution containing fumarase enzyme, showing metabolism of fumarate to malate. (c) Integrals of the fumarate and malate ^{13}C NMR signals normalized to 1 for the first fumarate signal, with the malate signals multiplied by 4 for clarity. The biochemical reaction is shown in the inset for clarity. (d) A comparison between thermal equilibrium ^{13}C NMR spectra for a purified and a control sample, acquired in an 11.7 T magnet. In the control sample spectrum some known resonances are labelled, with additional resonances likely present due to reaction side products. (e) A comparison between a control and a purified sample.